Application of MA-ATI SAR for Estimating the Direction of Moving Water Surface Currents in Pi-SAR2 Images

Takero Yoshida, *Member, IEEE*, Kazuo Ouchi, *Senior Member, IEEE*, and Chan-Su Yang, *Senior Member, IEEE*

***Abstract*—A multiaperture along-track interferometric synthetic aperture radar (MA-ATI SAR) theory was proposed to obtain velocity vectors of moving objects. This theory utilizes two antennas to estimate two velocity components (aft- and fore-looking directions) by multi/sublook processing. The moving direction can then be calculated by the two velocity components. Combining it with the conventional range velocity estimation, the velocity vector can be estimated. In order to validate its methodology, the present study applies MA-ATI SAR to airborne polarimetric interfereometric SAR-2 (Pi-SAR2) for estimating the directions of moving water surface currents of rivers. The results were in good agreement with the true moving directions. The estimated accuracy showed the direction error of approximately 20° for the three cases out of four. One case showed the higher error, since there may be complicated flow patterns. The findings of this study have implications for the applicability of the MA-ATI method to an airborne SAR system.**

***Index Terms*—Multiaperture along-track interferometric synthetic aperture radar (MA-ATI SAR), multi/sublook processing, velocity vector, water surface current.**

I. Introduction

SYNTHETIC aperture radar (SAR) is a promising method to observe Earth's surface while avoiding the impacts of weather and day/night conditions [1]. One of the applications of SAR is velocity measurements of moving targets using along-track interferometry (ATI) with multiple antennas, usually two antennas are utilized (fore- and aft-antennas). Several studies have been reported ATI SAR over oceanic scenes, including ocean currents [2]–[7] and waves [8], [9]. The baseline separation of antennas provides the phase difference between each antenna, and the phase difference is proportional to the velocity component of moving targets. However, the technique of ATI can measure only the velocity component in the line-of-sight view, i.e., the range direction. To estimate the velocity vector, dual-beam ATI SAR with a single pass [10], [11] was used by two squint beams in forward- and aft-looking directions. On the other hand, Ouchi *et al.* [12] proposed a multiaperture ATI SAR theory (MA-ATI SAR) as an improvement of ATI SAR to estimate the velocity vector. This method can estimate velocity vectors by applying multi/sublook processing to the SAR data obtained by two antennas with a single beam and single pass. The angle of the moving direction can be calculated by the two velocity components in the forward- and backward-looking directions. Combining the estimated direction with the conventional range velocity estimation by ATI SAR, the velocity vector can be ultimately estimated. The novelty of this method is its estimation of the velocity vector via two antennas without squinting the antenna beams; by contrast, the conventional technique required the dual-beam ATI SAR.

As an application of MA-ATI SAR, conventional ship detection uses algorithms that retrace bright points from the background ocean surface [13]–[17]; if these are combined with MA-ATI, they may provide useful information that could act as alternatives to autoindication of ship. In addition to this benefit, it is expected that the MA-ATI method could be used for monitoring ocean currents affecting localized oceanic environments. The information on ocean currents can also be used for fisheries or uses of ocean resources as well as understanding the marine environment.

In order to confirm the usage of MA-ATI SAR, Yoshida *et al.* [18] first validated the theory of MA-ATI with a numerical simulation. The principle of this numerical simulation is to calculate the SAR raw data [19], [20] from microwave backscattered signal with the physical optics scattering model [21] in the time domain. The water surface profile is generated with the Pierson-Moskowitz wave height spectrum [22]. Then, the multi/sublook processing is applied to each raw data to produce two sets of aft- and fore-looking single-look complex (SLC) images, followed by the direction estimation of the moving targets and currents. The results showed that the estimation accuracy of the direction of moving targets was within an error of 10° for estimating the angles of both moving targets and ocean currents. Additionally, the numerical simulation indicated that the accuracy depended on the azimuth beam width. The MA-ATI theory also implied that the accuracy of direction estimation

Manuscript received February 27, 2020; revised August 27, 2020 and February 14, 2021; accepted February 15, 2021. Date of publication February 17, 2021; date of current version March 8, 2021. This work was supported in part by the Grants-in-Aid Scientific Research of the Japan Society for the Promotion of Science (JSPS KAKENHI) under Grant JP20K14961 and in part by the Ministry of Oceans and Fisheries, South Korea, under the Projects entitled "Development of Satellite-based System on Monitoring and Predicting Ship Distribution in the Contiguous Zone" and "Technology Development for Practical Applications of Multi-Satellite Data to Maritime Issues." *(Corresponding author: Takero Yoshida.)*

Takero Yoshida and Kazuo Ouchi are with the Institute of Industrial Sciences, The University of Tokyo, Kashiwa-shi 277-8574, Japan (e-mail: tyoshida@iis.u-tokyo.ac.jp; ouchi.kazuo@gmail.com).

Chan-Su Yang is with the Korea Institute of Ocean Science & Technology, Yeongdo-gu 49111, South Korea (e-mail: yangcs@kiost.ac.kr).

Digital Object Identifier 10.1109/JSTARS.2021.3060008

can be increased if the azimuth beam width is increased. The numerical simulation results indicated that the difference between the estimated and correct angle correlates with a half of the subaperture azimuth beam angle. If half of the subaperture azimuth beam angle is greater than 1.25°, the estimation is accurate within the above-mentioned errors of moving angles.

To date, an airplane observation system has been used to operate ATI SAR, and could therefore be expected to be applied to MA-ATI because of its relatively large azimuth beam angles. As to spaceborne systems, two SARs in tandem [23], [24] may also be able to apply the MA-ATI method. In this article, we will show, following the previous simulation results [18], further validation using airborne SAR data acquired by Pi-SAR2 [25]. The Pi-SAR2 X-band system with along-track capabilities has been making land and ocean observations [26]. Additionally, the Pi-SAR2 L-band can also be used for land observations with cross-track measurements [27], [28]. The halved value of the subaperture azimuth beam angle of Pi-SAR2 is approximately 1.5°; thus, the observation system is considered feasible for MA-ATI SAR according to the findings of a previous simulation study [18].

In this study, MA-ATI SAR is first applied to a scene of water surface currents of river, and the estimated angle from MA-ATI is compared with the moving directional angle to show the applicability of the MA-ATI SAR theory with real airborne SAR images. In this analysis, two sets of images acquired by fore- and aft-antennas are prepared. Then, the sublook processing is applied to both sets of images. The forward- and backward-looking velocity components are obtained by interferometric phases. The direction of the moving target is then estimated by the absolute velocities in the forward- and backward-looking directions, which were obtained by comparing to the stationary pints such as land areas. Finally, the estimation is compared with the angles of river currents, which were determined via the SAR images. Through these results, we discuss the accuracy of estimating the moving angle.

The rest of this article is organized as following. The summary of the principal theory of MA-ATI SAR is given in Section II, followed by the results in Section III, with conclusions in Section IV.

II. Methodology

To apply the MA-ATI theory to SLC images, a sublook analysis was adopted. An image formed by a part of full bandwidth is called a sublook image. Sublook images, or subimages over ocean, have been used by several researchers [29], [30]. This study also applies the same processing method of the above works. Sublook images have a lower resolution and a different central frequency than those of full looks. More than two sublook images (e.g., four-looks or more) can be created to separate the bandwidth. Fig. 1 illustrates the multi/sublook processing technique applied to an SLC image. Note that the same processing method can also be adapted to SAR raw data by applying subreference signals.

Extractions of sublook images from SLC images are performed as detailed in the following steps. During the processing,

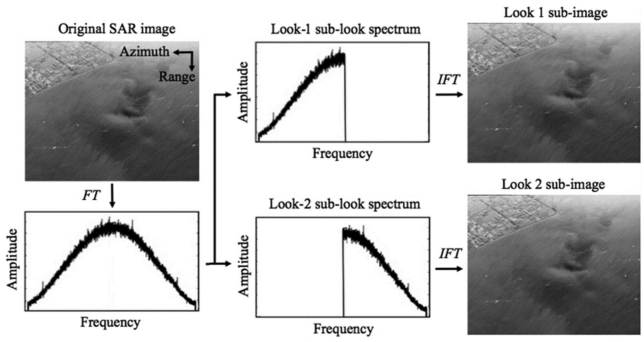

Fig. 1. Illustration of the multi/sublook processing method applied to MA-ATI SAR. An SLC image was FT, and the spectrum was divided into look-1 and 2 sublook spectra. Look-1 and 2 subimages were produced through an IFT of the corresponding spectra.

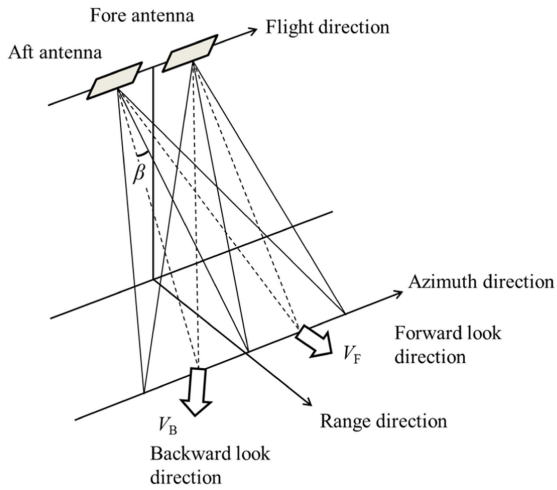

Fig. 2. Schematic of the forward- and backward-looking directions.

the original SLC image is Fourier transformed (FT) to produce a full-look image spectrum. Half of this spectrum is zero-padded and inverse FT (IFT), yielding a subimage, i.e., the look-1 forward-looking subimage in Fig. 1. Similarly, another half spectrum undergoes IFT to produce the look-2 backward-looking subimage.

Originally, multi/sublook images are produced by dividing the raw data into two or more subdata and processing each subdata with multi/sublook processing. The present processing method can be directly applied to SLC images without raw data. Additionally, it can also be applied to range directions, mainly because of the equalization of coarse azimuth resolution of spaceborne SARs with finer range resolution. In the present study, however, the sublook processing is applied to the azimuth resolution having the inter-look time difference.

By applying these steps to the original images acquired by fore- and aft-antennas, four subimage data sets can be obtained: two forward-looking and two backward-looking subimages. Using the four data sets, the phase differences between fore- and aft-antennas can be calculated for forward- and backward-looking directions. Fig. 2 depicts the schematic illustration of each

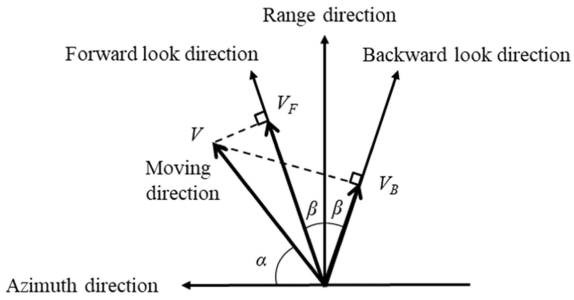

Fig. 3. Estimation of moving angle α, which is the direction of a moving target; V is the velocity vector, V_F and V_B are the velocity components in the forward- and backward-looking directions, respectively, and β is the angle of each looking direction.

looking direction. The forward-looking and backward-looking velocity components, V_F and V_B, respectively, can be obtained from the interferometric phases given by

$$\varphi_{F,\,B} = \frac{4\pi}{\lambda} V_{F,\,B} \sin\theta\, \Delta t \tag{1}$$

where φ_{F} and φ_{B} are the phases of the forward- and backward-looking interferograms, respectively, and λ is the radar wavelength. Δt is the effective time lag between the fore and aft antennas, and θ is the incidence angle. Here, the term of phase ambiguity is neglected for simplicity. Note that the ellipsoid, topography, and orbit error should be removed from (1) during satellite observations. However, this study analyzed the airplane SAR, and the above-mentioned effects were considered minimal. In addition, if the method is applied to ocean or water surfaces of rivers, the other phase contributions such as intrinsic phase velocity, Bragg waves, or the orbital motion of waves, must be removed or compensated. In this study, these parameters were ignored for simplicity.

Based on the theory of MA-ATI SAR [12], the geometry of our proposed method is depicted in Fig. 3. In Fig. 3, V is the velocity vector of a moving target with the direction movement of α. V_F and V_B are the velocity components in the forward- and backward-looking directions. β is the angle of each looking direction, namely half of the subaperture azimuth beam angle, which is also depicted in Fig. 2.

The velocity components, V_F and V_B, are expressed through the following equations from the geometry in Fig. 3:

$$V_F = V\sin(\alpha+\beta) \tag{2}$$

$$V_B = V\sin(\alpha-\beta). \tag{3}$$

Then, the angle of the moving target's direction, α, can be given by the geometrical relationship shown in Fig. 3. This relationship is written as the following equation:

$$\tan\alpha = \left(\frac{V_F+V_B}{V_F-V_B}\right)\tan\beta. \tag{4}$$

It can also be expressed as the interferometric phases by the following simple equation:

$$\tan\alpha = \left(\frac{\varphi_F+\varphi_B}{\varphi_F-\varphi_B}\right)\tan\beta. \tag{5}$$

TABLE I
SAR IMAGE SPECIFICATION

Scene ID	Obs20_00-00ssc_VVa, Obs20_00-00ssc_VVf
Acquisition time	August 23rd, 2011
Altitude	8917 m
Start near location	35:48:58, 139:54:47
Start far location	35:44:45, 139:54:40
End near location	35:48:59, 139:18:11
End far location	35:44:46, 139:18:11
Polarization	VV

Note that the phase angles in (5) are not absolute values, so that a reference phase of a stationary target is required to compute the absolute phase angles, in particular, for the airborne case, which may have phase differences due to drift angle of the airplane. Also, if we use (4), the velocities should be the absolute values to compare reference stationary points. In terms of phase unwrapping, the limitation is similar to the usual ATI method.

From these relationships, we can estimate the moving angle from two velocity components or interferometric phases. The velocity vector of moving targets can be derived by combining the moving angle with the range velocity component estimated by using the conventional ATI. In the analysis of Pi-SAR2 images, we used the above-mentioned equations to estimate the moving direction because the interferometric phases could be obtained directly from the sets of sublook complex images for fore- and aft-antennas.

In general, the phase difference between the forward- and backward-looking directions is similar because of the small β angle. However, the estimate will be less accurate if one of the directions is unwrapped. The ambiguous slant-range velocity for Pi-SAR2 is approximately 10–20 m/s [12], [25]. Targets moving faster than this velocity will not be detected due to phase unwrapping. However, water surface currents slower than 10–20 m/s could be detected. To avoid this problem, which is caused by phase unwrapping, this study adopted extended phase ranges, at -2π to 2π from $-\pi$ to π, depending on the distribution of phase differences. The details are described in the next section.

III. RESULTS AND DISCUSSION

The Pi-SAR2 X-band ATI SAR was used for the SAR images in this study. The images were provided by the National Institute of Information and Communications Technology[1]. Pi-SAR2 data for the Edo River in Japan were selected (see Fig. 4). As listed in Table I, the images were from fore- and aft-antennas (Scene ID: Obs20_00-00ssc_VVa and Obs20_00-00ssc_VVf).

Four points denote the targeted areas, and their pixel values are 100×100, as shown in Fig. 4. The target areas are equal to 30 m^2. This area was selected because we assumed that the average phases calculated by the relatively larger areas would be sufficient to retrieve the river current information while excluding other effects, such as surface roughness due to small waves.

[1][Online]. Available: https://pi-sar.nict.go.jp/

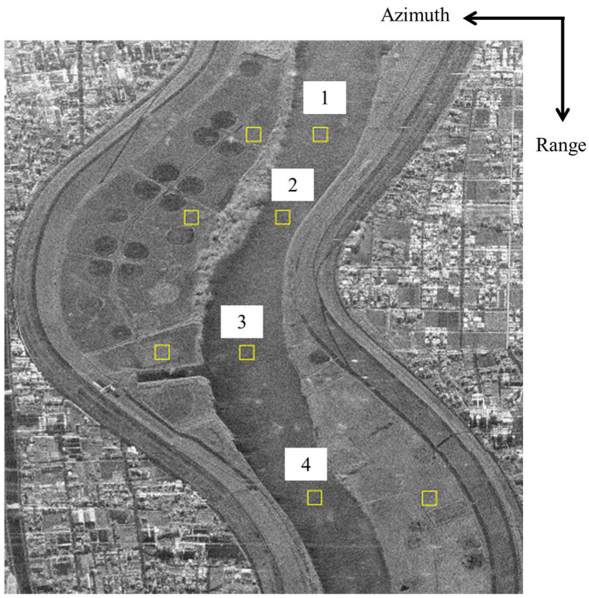

Fig. 4. Pi-SAR2 image of the Edo River in Japan. The rectangles are the areas analyzed for river and land on the same azimuth line. This figure is based on Pi-SAR2 image data by the National Institute of Information and Communications Technology.

In the case of Pi-SAR2, β—the key factor for accurate velocity vector measurements—is approximately 1.5° [12]. This angle is generally wider than that of the spaceborne SARs. If the angle of β is narrow, the differences between the two velocities of forward- and backward-looking directions as shown in Fig. 3 will be quite similar, resulting in less accurate measurements. Thus, in this study, the data obtained by the airborne Pi-SAR2 with bigger β angles are used for the initial validation.

As a first stage, four sets of phases of sublook images were computed. Then the phase differences, i.e., interferometric phases, in the forward- and backward-looking directions were obtained. The phase differences both river and land, which locates the same azimuth line with that of river, were obtained. The absolute velocities in the forward- and backward-looking directions were calculated by comparing them. Finally, the moving directions were estimated from the relationship of (4).

Figs. 5 –8 are the results of interferometric phases. The phases were likely to fluctuate and potentially resulted in estimation errors. Furthermore, the movement of the river resulted in a smearing of the image. Thus, the phase was likely to have fluctuated due to the shape and motion of the target. The phase variation could therefore potentially result in errors in estimations of the moving angle via MA-ATI.

It can also be seen that the phase differences over stationary land are nonzero. This is because of the drift angle of the unstable airborne platform. To minimize the effect of the drift angle, we calculated the absolute phase differences of the rivers with respect to those of the land. The problem of the drift angle was also reported by Kojima *et al.* [25].

To estimate the accurate movement angle via MA-ATI, determining the proper method to obtain the representative phase is an important objective of our analysis. In this study, the

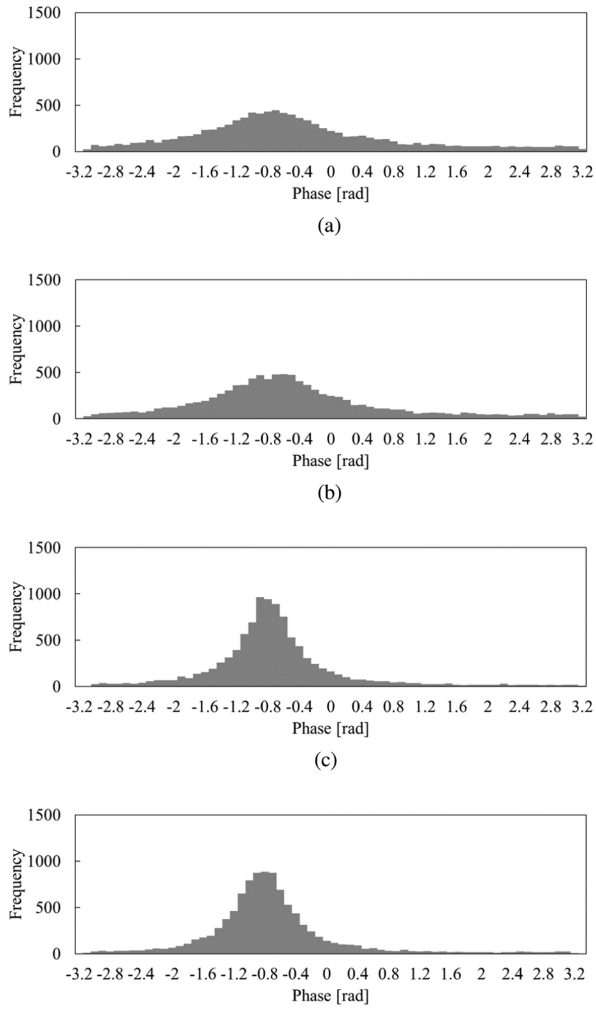

Fig. 5. Histograms of interferometric phases. (a) φ_{F} and (b) φ_{B} for No. 1 on the river, and (c) φ_{F} and (d) φ_{B} for No. 1 on land.

TABLE II
ANGLE ESTIMATION RESULTS

No.	Angles of river side	Average v_{F} (m/s)	Average v_{B} (m/s)	Estimated angle	Difference
1	65-72°	0.88463	0.88777	86.1°	14.1-21.1°
2	52-65°	0.46406	0.47416	67.7°	2.7-15.7°
3	114-117°	0.63568	0.51783	165.6°	48.6-51.6°
4	116-122°	1.42727	1.30381	149.9°	27.9-33.9°

representative phases were calculated based on the histograms of varied phases. Each histogram has a peak within the corresponding distribution. In our analysis, the average values of the interferometric phases were calculated for both rivers and lands. We considered the average values as the representative phases; hence, by translating them into absolute velocities by comparing to those of land, and then inserting these values into (4), the estimated movement angles could be calculated. The estimated results are also shown in Table II.

To survey the correct view angles of the river, we assumed that the water flow in the center of the river within the analytical

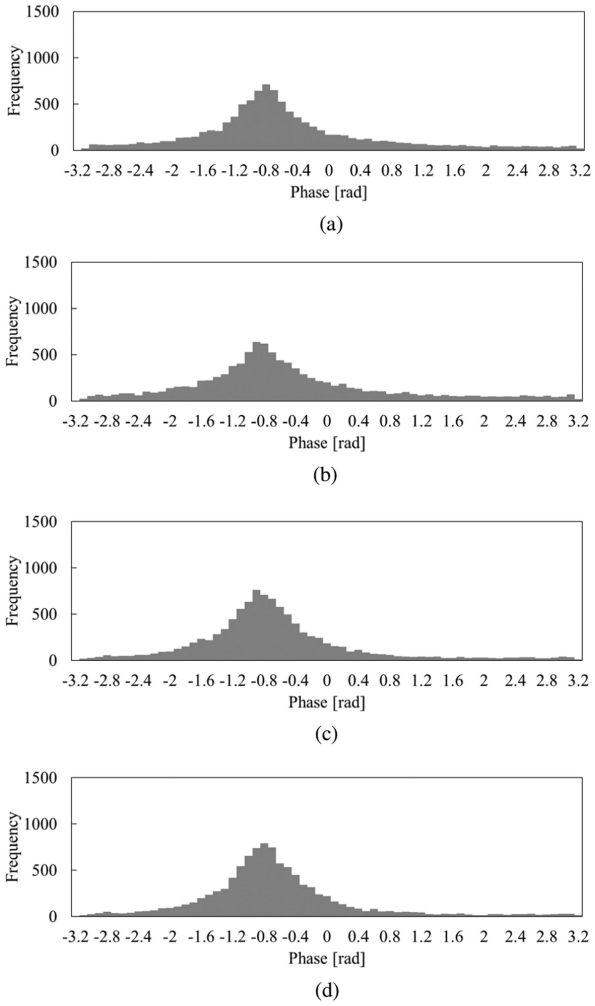

Fig. 6. Histograms of interferometric phases. (a) φ_{F} and (b) φ_{B} for No. 1 on the river, and (c) φ_{F} and (d) φ_{B} for No. 2 on land.

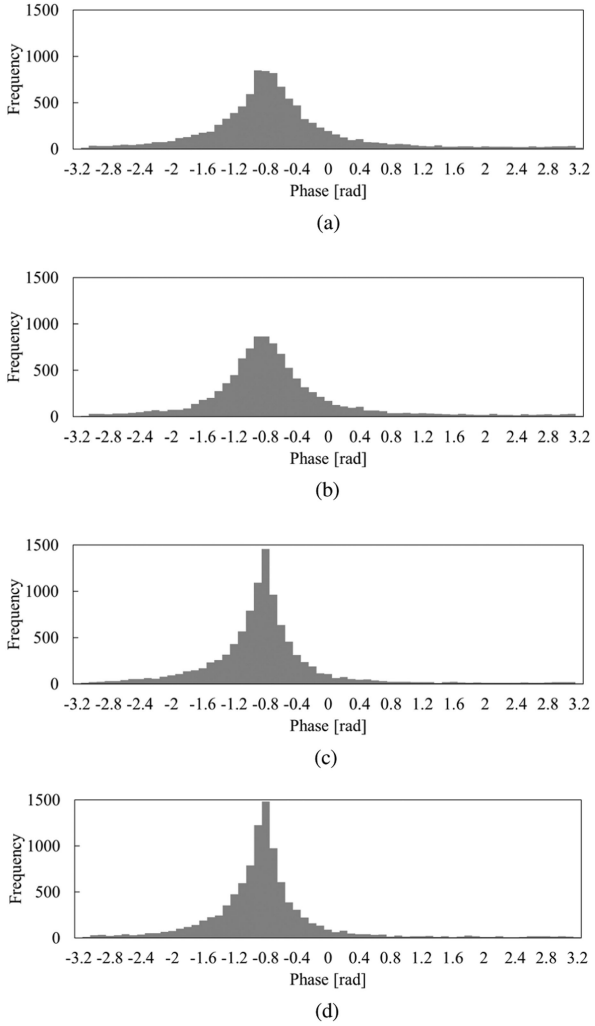

Fig. 7. Histograms of interferometric phases. (a) φ_{F} and (b) φ_{B} for No. 1 on the river, and (c) φ_{F} and (d) φ_{B} for No. 3 on land.

area was uniform along the line of the riverside. Thus, the correct angle of the river was calculated from the angle of both riverside lines. We consider that this assumption is reasonable in obtaining correct water current information, although the true currents cannot be determined using this assumption alone.

Based on this hypothesis, the estimated directions of river flows were listed in Table II. The differences between the estimated and reference angles were 14.1–21.1°, 2.7–15.7°, 48.6–51.6°, and 27.9–33.9° for Nos. 1–4, respectively. The average value of all measurement errors was 27°. Especially, the No. 3 has the largest error. The reason may be because the river width of this area is larger than the others as a meeting point of different flow directions, and as such the water flow is close to a turbulent flow in comparison with the other areas.

When we remark on the width of spectral peaks, Nos. 1 and 4 (see Figs. 5 and 8) showed broad spectra at the river. They showed the spectra contain multidirectional water surface flows. In contrast, No. 2 (see Fig. 6) had narrower spectra at the river, it is because the width of river is narrower than the other points, and it can result in uniform flow along with the riverside. Accordingly, the No. 2 was the best estimation in all results. In the case of No. 3 (see Fig. 7), the spectral peaks of river are also not broad. Here, the velocities may be mixed due to the turbulent flow as we mentioned above, then the flow may not be parallel to the riverside at this area.

If we exclude No. 3 in the total average value of the estimation, it will be roughly 19°. Nevertheless, this kind of error of approximately 20° is considered acceptable when estimating the directions of water surface currents, in particular for the case of vast ocean currents. From the present results, it can be stated that the MA-ATI method is capable of estimating the direction of water flow by airborne ATI, and potential applications to ocean currents. Further, together with the current velocity measured by the conventional ATI method, the MA-ATI can be extended to the estimation of velocity vectors.

It should be noted that the scattering mechanism of the surface of the water dominant by the Bragg waves generated by wind. This means that a received signal contains the velocity component of the intrinsic phase velocity of the Bragg waves. This factor may, therefore, affect angular estimations of river flow. In

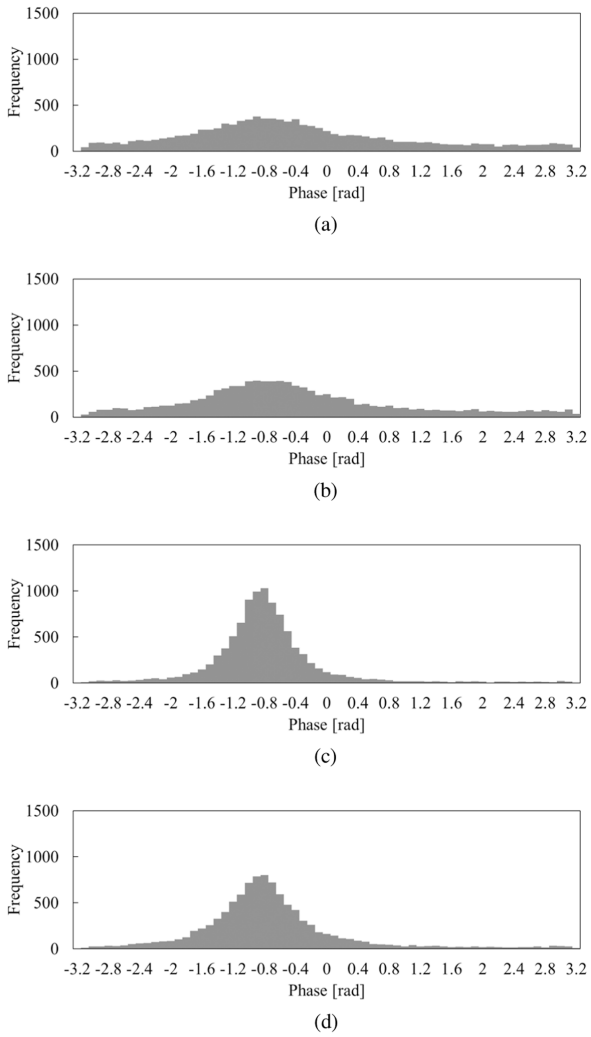

Fig. 8. Histograms of interferometric phases. (a) φ_{F} and (b) φ_{B} for No. 1 on the river, and (c) φ_{F} and (d) φ_{B} for No. 4 on land.

addition, we hypothesized that the water surfaces were moving in the same direction in each sublook; specifically, the moving targets were assumed as moving in a uniform direction during the SAR observation. If the synthetic aperture time is long enough so that the directions of the moving targets change during the integration time. Then, the estimation accuracy may decrease. Further, if a histogram is excessively varied and it does not show a single peak, the current method cannot accurately estimate the directions of moving targets. Speckle and system noise may also impact estimation accuracy. In this article, we used the average values of the histograms to include the water surface flow as expressed the width of spectral peaks. However, the width of spectral peaks also can be used for the estimation. This might be helpful for further discussion to improve the MA-ATI method as a future task.

IV. Conclusion

This study described the applications of the MA-ATI SAR theory to Pi-SAR2 images of a river. The two velocity components of the water flow in the forward- and backward-looking directions were analyzed from their interferometric phases by adopting sublook processing. Then, the directions of surface currents over the river were estimated. The results showed that the mean direction difference except one (No. 3) out of 4 sample areas was approximately 20°. The larger error of No. 3 area compared with the others is due possibly to the complicated flow patterns that may not be parallel to the riverside.

The velocity vector can be estimated via the range velocity component determined by the conventional ATI and the moving directional angle by the MA-ATI. The directions of water flow measured in the present study were between 52° and 122° from the azimuth direction. The estimated velocity vector contains small errors depending on the flow directions. If, however, the flow directions are close to the azimuth direction, the velocity components of the forward and backward looks are small, resulting in decreasing the estimation accuracy. Nevertheless, the MA-ATI estimation showed an acceptable accuracy in the present study.

The findings of this study have implications for the applicability of the MA-ATI method to an airborne SAR system as well as spaceborne SARs. Applications can also be extended to estimating the velocity vector of ocean currents although the effects of waves and winds should be discussed prior to MA-ATI's application to ocean currents.

Acknowledgment

Pi-SAR2 images analyzed in this work were provided by the National Institute of Information and Communications Technology (https://pi-sar.nict.go.jp/), Japan.

References

[1] K. Ouchi, "Recent trend and advance of synthetic aperture radar with selected topics," *Remote Sens.*, vol. 5, pp. 716–807, 2013.
[2] R. M. Goldstein and H. A. Zebker, "Interferometric radar measurement of ocean surface currents," *Nature*, vol. 328, pp. 707–709, 1987.
[3] R. M. Goldstein, T. P. Barnett, and H. A. Zebker, "Remote sensing of ocean currents," *Science*, vol. 246, pp. 1282–1285, 1989.
[4] R. Romeiser, "Current measurements by airborne along-track InSAR: Measuring technique and experimental results," *IEEE J. Ocean. Eng.*, vol. 30, no. 3, pp. 552–569, Jul. 2005.
[5] R. Romeiser *et al.*, "Current measurements by SAR along-track interferometry from a space shuttle," *IEEE Trans. Geosci. Remote Sens.*, vol. 43, no. 10, pp. 2315–2324, Oct. 2005.
[6] R. Romeiser, S. Suchandt, H. Runge, U. Steinbrecher, and S. Grünler, "First analysis of TerraSAR-X along-track InSAR-derived current fields," *IEEE Trans. Geosci. Remote Sens.*, vol. 48, no. 2, pp. 820–829, Feb. 2010.
[7] R. Romeiser, "The future of SAR-based oceanography: High-resolution current measurements by along-track interferometry," *Oceanography*, vol. 26, no. 2, pp. 92–99, 2013.
[8] P. W. Vachon, J. W. M. Campbell, A. L. Gray, and F. W. Dobson, "Validation of along-track interferometric SAR measurements of ocean surface waves," *IEEE Trans. Geosci. Remote Sens.*, vol. 37, no. 1, pp. 150–162, Jan. 1999.
[9] D. Kim, W. M. Moon, D. Moller, and D. A. Imel, "Measurements of ocean surface waves and currents using L- and C-band along-track interferometric SAR," *IEEE Trans. Geosci. Remote Sens.*, vol. 41, no. 12, pp. 2821–2832, Dec. 2003.
[10] S. J. Frasier and A. J. Camps, "Dual-beam interferometry for ocean surface current vector mapping," *IEEE Trans. Geosci. Remote Sens.*, vol. 39, pp. 401–414, Feb. 2001.

[11] S. Wollstadt, P. López-Dekker, F. De Zan, and M. Younis, "Design principles and consideration for spaceborne ATI SAR-based observations of ocean surface velocity vectors," *IEEE Trans. Geosci. Remote Sens.*, vol. 55, pp. 4500–4519, Aug. 2017.
[12] K. Ouchi, T. Yoshida, and C.-S. Yang, "A theory of multi-aperture along-track interferometric synthetic aperture radar (MA-ATI SAR)," *IEEE Geosci. Remote Sens. Lett.*, vol. 16, no. 10, pp. 1565–1569, Oct. 2019.
[13] W. Ao, F. Xu, Y. Li, and H. Wang, "Detection and discrimination of ship targets in complex background from spaceborne ALOS-2 SAR images," *IEEE J. Sel. Top. Appl. Earth Obs. Remote Sens.*, vol. 11, no. 2, pp. 536–550, Feb. 2018.
[14] S. Brusch, S. Lehner, T. Fritz, M. Soccorsi, A. Soloviev, and B. van Schie, "Ship surveillance with TerraSAR-X," *IEEE Trans. Geosci. Remote Sens.*, vol. 49, pp. 1092–1103, Mar. 2011.
[15] A. Marino, M. J. Sanjuan-Ferrer, I. Hajnsek, and K. Ouchi, "Ship detection with spectral analysis of synthetic aperture radar: A comparison of new and well-known algorithms," *Remote Sens,* vol. 7, no. 5, pp. 5416–5439, 2015.
[16] K. Ouchi, S. Tamaki, H. Yaguchi, and M. Iehara, "Ship detection based on coherence images derived from cross correlation of multilook SAR images," *IEEE Geosci. Remote Sens. Lett.*, vol. 1 no. 3, pp. 184–187, Jul. 2004.
[17] S.-I. Hwang and K. Ouchi, "On a novel approach using MLCC and CFAR for the improvement of ship detection by synthetic aperture radar," *IEEE Geosci. Remote Sens. Lett.*, vol. 7, no. 2, pp. 391–395, Apr. 2010.
[18] T. Yoshida, K. Ouchi, and C. Yang, "Validation of MA-ATI SAR theory using numerical simulation for estimating the direction of moving targets and ocean currents," *IEEE Geosci. Remote Sens. Lett.*, to be published.
[19] T. Yoshida and C. K. Rheem, "SAR image simulation in time domain for moving ocean surfaces," *Sensors*, vol. 13, pp. 4450–4467, 2013.
[20] T. Yoshida and C. K. Rheem, "Time-domain simulation of along-track interferometric SAR for moving ocean surfaces," *Sensors*, vol. 15, pp. 13644–13659, 2015.
[21] S. Silver, *Microwave Antenna Theory and Design*. London, U.K.: Peter Peregrinus, pp. 144–168, 1949.
[22] W. J. Pierson and L. Moskowitz, "A proposed spectral form for fully developed wind sea based on the similarity theory of S. A. Kitaigorodskii," *J. Geophys. Res.*, vol. 69, pp. 5181–5190, 1964.
[23] R. Romeiser, H. Runge, S. Suchandt, R. Kahle, C. Rossi, and P. S. Bell, "TerraSAR-X and TanDEM-X along-track interferometry and doppler centroid analysis," *IEEE Trans. Geosci. Remote Sens.*, vol. 52, no. 5, pp. 2759–2772, May 2014.
[24] S. Buckreuss *et al.*, "Ten years of TerraSAR-X operations," *Remote Sens*, vol. 10, 2018, Art. no. 873.
[25] S. Kojima, T. Umehara, J. Uemoto, T. Kobayashi, M. Satake, and S. Uratsuka, "Development of PiSAR2 along-track interferometric SAR system," in *Proc. IEEE Int. Geosci. Remote Sens. Symp.*, 2011, pp. 3159–3162.
[26] A. Nadai, T. Umehara, S. Kojima, and J. Uemoto, "Ocean wave measurement using synthetic aperture radar cross-track interferometry," in *Proc. Int. Symp. Antennas Propag*, 2016, pp. 7965–7967.
[27] R. B. Thapa, M. Watanabe, M. Shimada, and T. Motohka, "Examining high-resolution PiSAR-L2 textures for estimating tropical forest carbon stocks," *IEEE J. Sel. Top. Appl. Earth Obs. Remote Sens.*, vol. 9, no. 7, pp. 3202–3209, Jul. 2016.
[28] M. Shimada, *Imaging From Spaceborne and Airborne SARs, Calibration, and Applications*. Orlando, FL, USA: CRC Press, pp. 5–15, 2018.
[29] C. Brekke, S. N. Anfinsen, and Y. Larsen, "Subband extraction strategies in ship detection with the subaperture cross-correlation magnitude," *IEEE Geosci. Remote Sens. Lett.*, vol. 10, no. 4, pp. 786–790, Jul. 2013.
[30] A. Renge, M.-D. Graziano, and A. Moccia, "Segmentation of marine SAR images by sublook analysis and application to sea traffic monitoring," *IEEE Tans. Geosci. Remote Sens.*, vol. 57, no. 3, pp. 1463–1477, Mar. 2018.

Takero Yoshida (Member, IEEE) received the Ph.D. degree in environmental studies from the Department of Ocean Technology, Policy and Environment, The University of Tokyo, Tokyo, Japan, in 2013.

He is an Assistant Professor with the Institute of Industrial Science, The University of Tokyo, since 2016. His research activities are in the fields of ocean monitoring, marine environmental impact assessments, SAR image analysis in oceanic scenes, and numerical simulation of electromagnetic scattering from ocean surfaces.

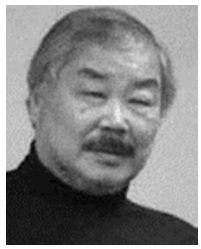

Kazou Ouchi (Senior Member, IEEE) received the Ph.D. degree with the Department of Physics, Imperial Collage of Science and Technology, University of London, England, U.K., in 1981.

He was a Research Assistant with Imperial Collage, a Research Associate in King' Collage, and a Research Fellow with Imperial Collage, University of London from 1980 to 1996. He was a Professor with the Department of Environmental Studies, Hiroshima Institute of Technology, Hiroshima, Japan, in 1996–1999. He was a Professor with the Department of Environmental Systems Engineering, Kochi University of Technology, Kochi, Japan, in 1999–2006. He was a Professor with the Department of Computer Science, National Defense Academy, Kanagawa, Japan, in 2006–2013. After retirement from NDA in March 2013, he has been a Research Scientist of the Brain Pool Program with the Korea Institute of Ocean Science and Technology, Jindo, South Korea. He was a Senior Consulting Manager with IHI Corp., Tokyo, Japan, from 2015 to 2020. His research interests include SAR/InSAR/PolSAR systems and applications to land and ocean, EM scattering, and microwave/optical remote sensing.

Chan-Su Yang (Senior Member, IEEE) received the Ph.D. degree in coastal application studies of satellite remote sensing from the Department of Civil Engineering from Tohoku University, Sendai, Japan, in 2001.

He is a Principal Research Scientist with the Korea Institute of Ocean Science and Technology, Busan, South Korea. He is also a Professor with Korea University of Science & Technology, Daejeon and School of Ocean Science and Technology, KMOU, Busan, South Korea. His research interests include the fields of satellite ocean monitoring and SAR applications.